Contrib Mineral Petrol (2006) 152:375–385
DOI 10.1007/s00410-006-0113-4

ORIGINAL PAPER

Zr-in-rutile thermometry in blueschists from Sifnos, Greece

Frank S. Spear · David A. Wark · John T. Cheney · John C. Schumacher · E. Bruce Watson

Received: 20 December 2005 / Accepted: 26 May 2006 / Published online: 21 July 2006

Abstract Zr-in-rutile thermometry on samples of blueschist from Sifnos, Greece, yields temperatures that reflect progressive crystallization of rutile from ca. 445 to 505°C with an analytical precision of + 18/–27 and ± 10°C using the electron microprobe and ± 1.5–3.5°C using the ion microprobe. Individual grains are generally homogeneous within analytical uncertainty. Different grains within a single sample record temperature differences as large 55°, although in most samples the range of temperatures is on the order of 25°. In several samples, Zr-in-rutile temperatures from grains within garnet are lower than temperatures from matrix grains, reflecting growth of rutile with increasing temperature of metamorphism. Although the specific rutile-producing reactions have not been identified, it is inferred that rutile grows from either continuous reaction involving the breakdown of lower grade phases (possibly ilmenite), or from pseudomorph reactions involving the breakdown of relic igneous precursors at blueschist-facies conditions. No systematic variation in rutile temperatures was observed across the blueschist belt of northern Sifnos, consistent with the belt having behaved as a coherent block during subduction.

Keywords Rutile · Thermometry · Blueschist · Cyclades · Sifnos

Communicated by T.L. Grove

F. S. Spear (✉) · D. A. Wark · E. B. Watson
Department of Earth and Environmental Sciences,
Rensselaer Polytechnic Institute, Troy, NY 12180, USA
e-mail: spearf@rpi.edu

J. T. Cheney
Department of Geology, Amherst College,
Amherst, MA 01002, USA

J. C. Schumacher
Department of Earth Sciences, University of Bristol,
Bristol BS8 1RJ, UK

Introduction

The recycling of material between the crust and the mantle occurs at subduction zones and the thermal structure of subduction zones is an important constraint on the mechanisms by which these processes occur. Recently, several calibrations of a new Zr-in-rutile thermometer have been proposed, which have the potential of permitting far more precise temperature estimates of blueschist metamorphism than have been previously possible (e.g. Zack et al. 2004; Degeling 2002; Watson et al. 2006).

The purpose of this paper is to present the first systematic application of the Zr-in-rutile thermometer to blueschist-facies rocks. The goal is to determine whether the thermometer behaves in a sufficiently systematic way to provide meaningful, interpretable, and useful temperature constraints on blueschist metamorphism. For example, is there a sufficient approach to equilibrium during metamorphism that the thermometer records systematic temperatures? Does rutile grow by discontinuous or continuous reaction? What part of a rock's history does rutile thermometry record? Rutile thermometry can potentially provide sufficiently precise and meaningful temperature estimates to enable differentiating otherwise similar blueschist tectonic blocks in more complex terrains.

The results of this study do indicate that rutile thermometry should enjoy fruitful application to unraveling tectonic problems in blueschist terranes, and such a study is currently underway on the complex mélanges of Syros Island also in the Aegean.

Geologic setting

Samples selected for this study are from the blueschist to eclogite facies rocks in the northern part of the island of Sifnos, Cyclades, Greece (Fig. 1). Sifnos is comprised of two lithotectonic facies, a northern predominantly blueschist and marble belt and a southeastern belt of predominantly greenschist facies overprinted blueschists. On Sifnos the blueschists and greenschists are separated by a relatively sharp boundary. This boundary has been interpreted by Schliestedt and Matthews (1987) as resulting from fluid flow upward to the main marble unit. They argue that this marble acted as an impermeable layer that protected the overlying blueschists from rehydration. Alternatively, Avigad (1993) has suggested that the boundary is a low angle tectonic surface and that the greenschist facies overprinting occurred prior to juxtaposition of the two domains. In this model, the high-pressure rocks are thought to have been uplifted to shallow levels prior to assembly and thus preserved. Wijbrans et al. (1993) have suggested that delamination of lighter supracrustal rocks proximal to active subduction provided the cooling mechanism to preserve the blueschists and eclogites. In particular,

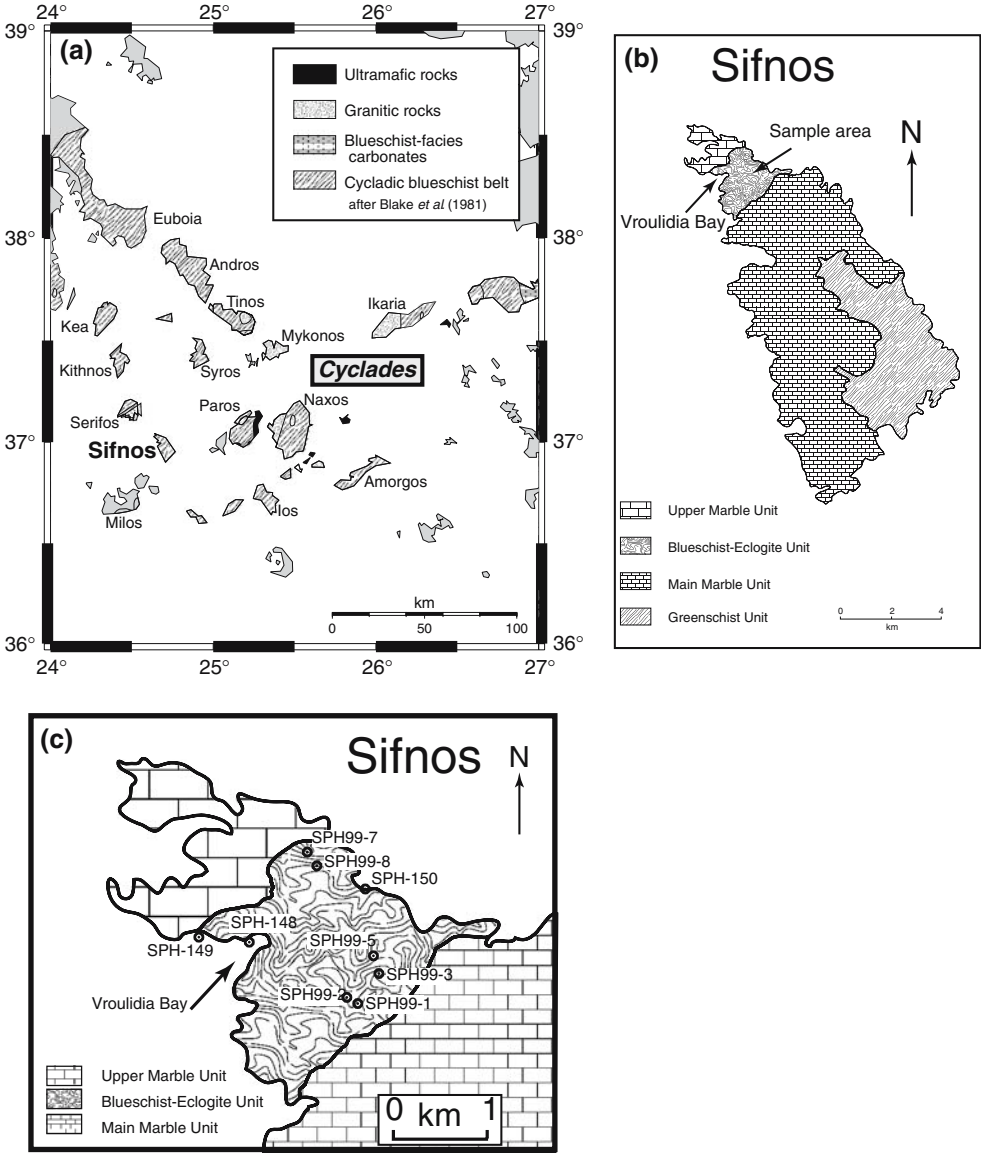

Fig. 1 Maps showing location of study area and samples. **a** Map of the Cyclades, Greece showing location of Sifnos (after Blake et al. 1981). **b** Geologic sketch map of Sifnos after Matthews and Schliestedt (1984). **c** Enlargement of the northern part of Sifnos showing sample locations

reversal of movement along subduction zone faults exhumed deeply buried (> 50 km) rocks. Thus, the nature of the contact between these units has been attributed to a fluid-infiltration front, a thrust fault, or a low-angle normal fault (for an excellent discussions and summaries of the geologic setting see Trotet et al. 2001a, b; Forster and Lister 2005).

The blueschists and eclogites of northern Sifnos were chosen for our initial study because previous work on these rocks (Matthews and Schliestedt 1984; Schliestedt 1986; Schliestedt and Matthews 1987; Schliestedt et al. 1987; Okrusch and Bröcker 1990; Trotet et al. 2001a, b; Schmädicke and Will 2003; Forster and Lister 2005) have documented that a wide range of bulk chemical compositions have given rise to a range of mineral assemblages representing a close approach to chemical equilibrium. The rocks are isoclinally folded and extensively sheared and flattened. Four generations of deformation have been recognized in terms of fabric and porphyroblast relations in rocks from Sifnos (Lister and Raouzaios 1996). Furthermore, the similarity of lithology and metamorphic histories suggests that these rocks form a coherent block that was metamorphosed under the same conditions throughout their history, thus avoiding possible complications due to the presence of different tectonic blocks with differing metamorphic histories.

The study suite consists of 12 samples from nine localities (Fig. 1) comprising both metapelites and metabasites (Table 1). Most of the sample localities are from relatively fresh outcrops along the main northern road of Sifnos; the other localities are all on the wave cut exposures along the coast. As shown in Table 1, the metapelites contain various proportions of garnet, phengite, paragonite, glaucophane, and quartz, with some samples containing epidote, chloritoid, and/or jadeite. Most metapelites contain ''clots'' of what may be pseudomorphs comprised predominantly of albite and magnetite, in some cases with minor glaucophane and epidote. These occur only in the matrix and are likely a manifestation of retrograde alteration. All samples of metapelite contain rutile and zircon both in the matrix and within garnet. Metabasites are comprised of garnet + omphacite + glaucophane ± epidote + paragonite ± phengite ± quartz ± ankerite + sphene + zircon. Rutile typically occurs only as inclusions within garnet whereas sphene is present in the matrix of the metabasites.

Most previous workers have concluded that the Sifnos blueschist–eclogite terrain has experienced a clockwise *P–T* path with maximum *P–T* conditions of 12–18 kbar and ca. 475°C (e.g. Schliestedt 1986; Matthews and Schliestedt 1984) although some higher

Table 1 Mineral assemblages in blueschist samples from Sifnos, Greece

Sample	Rock type	Minerals present	Comments
SPH99-1c	Metapelite	Grt + Phn + Pg + Qtz + Rt + Zrn + Gln + Ep + (Ab + Mt)	Ab + Mt ''clots'' are pseudomorphs
SPH99-2	Metapelite	Grt + Phn + Pg + Cld (in Grt) + Qtz + Rt + Zrn + Gln + Ep + (Ab + Mt)	Ab + Mt ''clots'' are pseudomorphs
SPH99-3	Metapelite	Grt + Phn + Pg + Cld (in Grt) + Qtz + Rt + Zrn + Ep + (Ab + Mt)	Ab + Mt ''clots'' are pseudomorphs
SPH99-5	Metapelite	Grt + Phn + Pg + Cld (in Grt) + Qtz + Rt + Zrn + Gln + Ep + (Ab + Mt)	Ab + Mt ''clots'' are pseudomorphs; Clinozoisite lineation inside garnet
SPH99-7	Metabasite	Grt + Jd + Gln + Ep + Rt + Sph + Pg + Phn + Qtz + Zrn	Rutile in garnet only; sphene in matrix
SPH99-8a	Metapelite	Grt + Phn + Pg + Qtz + Rt + Zrn + Gln + Ep + (Ab + Mt)	Ab + Mt ''clots'' are pseudomorphs
SPH99-8b	Metapelite	Grt + Phn + Pg + Omp (in Grt) + Qtz + Rt + Zrn + Gln + Ep + (Ab + Mt)	Ab + Mt ''clots'' are pseudomorphs
SPH-148a	Metabasite	Grt + Omp + Gln + Ep + Rt + Sph + Pg + Phn + Qtz + Zrn + Ank	Rutile in garnet only; sphene in matrix
SPH-148c	Metabasite	Grt + Omp + Gln + Ep + Rt + Sph + Pg + Phn + Zrn + Ank	Rutile in garnet only; sphene in matrix
SPH-149c	Metabasite	Grt + Omp + Gln + Ep + Rt + Sph + Pg + Phn + Qtz + Zrn	Rutile in garnet only; sphene in matrix
SPH-149d	Metapelite	Grt + Jd + Gln + Rt + Pg + Phn + Chl + Qtz + Zrn	Pseudomorph clusters of Rt + Zrn + silicates
SPH-150	Metapelite	Grt + Phn + Pg + Qtz + Rt + Zrn + Gln + (Ab + Mt) + Ank	Ab + Mt ''clots'' are pseudomorphs

Abbreviations: *Grt* garnet, *Qtz* quartz, *Phn* phengite, *Pg* paragonite, *Gln* glaucophane, *Omp* omphacite, *Jd* jadeite, *Rt* rutile, *Zrn* zircon, *Ab* albite, *Mt* magnetite, *Cld* chloritoid, *Ep* epidote, *Sph* sphene, *Ank* ankerite, *Chl* chlorite

temperature estimates have been proposed, for example up to 580°C (Trotet et al. 2001a) and 600°C (Schmädicke and Will 2003).

Methods

Chemical compositions were obtained using a Cameca SX-100 electron microprobe equipped with four large PET crystals (LPET) and flow detectors using P-10 gas, two of which operate at 1 atm. (LP) and two of which operate at 3 atm. (HP). Standards were synthetic zircon (for Zr) and rutile (for Ti). Zr was standardized at a current of 10 nA to avoid energy shift in the PHA due to different count rate between the standard and unknown.

Unknowns were analyzed using three different analysis protocols. Initially, Zr was analyzed at a current of 100 nA and counting times of 120 s on peak and 60 s each on the high and low background position. Later a current of 200 nA was found to cause negligible sample damage and counting times of 120 and finally 200 s on peak were used in order to improve counting statistics. Using this last analysis protocol, the Poisson precision for the LP and HP spectrometers is ca. 15 and 11 ppm, respectively. Results from the four spectrometers were averaged using weights proportional to the relative sensitivities of each spectrometer providing single spot precisions of approximately 13, 9, and 7 ppm for the three analytical protocols. The composition and accompanying errors are shown for each analysis in Table 2.

Trace element X-ray maps were collected on several samples for the elements Ti, Zr, Ce, P, and Y using a beam current of ca. 200 nA, dwell times of 10–50 ms, and a nominal step size of 15–20 μm with the beam defocused to ca. 20 μm. In this way large areas could be mapped for detection of small grains that contain the elements of interest. In particular, this method permitted easy identification of all of the rutile crystals of diameter larger than ca. 5 μm in the sample, and permitted ready identification of zircon (as well as apatite and allanite).

Two spot analyses were collected using the Cameca IMS 3f ion microprobe at Woods Hole Oceanographic Institute using a current of 2 nA and a spot size of 8–12 μm. Counts were collected on masses ^{90}Zr and ^{49}Ti and compared against a synthetic rutile standard with a concentration of 7,487 ppm Ti as determined by electron microprobe analysis. A value of ^{90}Zr/^{49}Ti = 0.0645 was determined on the standard and the correlation between this ratio and concentration was assumed to be linear. Unknown counts were collected in four magnet cycles of 10 s each. Total analysis time per spot was approximately 2 min. The Poisson precision using this analytical protocol was approximately ± 1 ppm Zr.

The three calibrations of the Zr-in-rutile thermometer are plotted in Fig. 2 for comparison:

Degeling (2002):

$$T_K = \frac{89297.49 + 0.63(P_{\text{bar}} - 1)}{R \ln\left[\frac{8.76\times10^7}{\text{Zr}_{\text{ppm}}}\right] + 33.46}$$

Zack et al. (2004):

$$T_C = 127.8 \ln(\text{Zr ppm}) - 10$$

Watson et al. (2006):

$$T_K = \frac{4470}{7.36 - \log_{10}(\text{Zr}_{\text{ppm}})}$$

The Degeling (2002) calibration is experimentally determined at temperatures above 1,000°C whereas the Watson et al. (2006) calibration is both experimental (at high temperature) and constrained by natural data at lower temperature. Errors associated with the ca. 500°C extrapolation of the Degeling (2002) equation from the high-temperature calibration range to the lower temperatures of blueschist conditions more than accounts for the 30–40° difference shown in Fig. 2 for temperatures calculated using these two thermometers. Zack et al. (2004) calibration regresses Zr concentration against T rather than $1/T$ so the temperature dependence is somewhat different from the other two, and the calibration predicts negative temperatures for Zr concentrations below ca. 1 ppm. Only the Degeling (2002) calibration specifically accounts for pressure and the calibrated effect is on the order of 4–5 deg/kbar (i.e. calculated temperature is on the order of 50° higher at 20 kbar than at 10 kbar). In this study the experimental calibration of Watson et al. (2006) was used, although the same systematics, but at higher temperatures, would be recorded using the calibration of Degeling (2002).

Analytical precision is plotted in Fig. 2 for the calibration of Watson et al. (2006) by propagating the electron microprobe Poisson statistics of ± 7 ppm through the thermometer. At 500°C the precision is approximately ± 10°C and at 450°C the precision is + 18/–27°C. A Zr concentration of 7 ppm corresponds to a temperature of 408°C, so this represents the lower limit of practical application of this thermometer using the electron microprobe for analysis. The temperature precision obtained from propagating the ± 1 ppm Poisson statistics of the IMS 3f is on the order of 1.5°C

Table 2 Zr in rutile analyses for blueschist samples from Sifnos, Greece

1	2 Grain	3 No. of spots[a]	4 Zr ppm	5 1σ (SD) [b]	6 Exp. SD [c]	7 1σ SE	8 T (°C)	9 1σ (SE)[d]	10 Notes
SPH99-1c	1	11	**19**	**8**	**9**	**3**	**463**	**9**	Matrix
	2	8	29	12	9	5	487	9	Matrix
	3	7	**34**	**6**	**9**	**4**	**496**	**7**	Matrix
	4	5	40	11	9	5	505	7	Matrix: garnet rim
	5	3	**18**	**9**	**9**	**5**	**460**	**14**	Inclusion: garnet
	6	5	**23**	**8**	**9**	**5**	**475**	**11**	Inclusion: garnet
	7	10	19	10	9	4	465	10	Inclusion: garnet
SPH99-2	1	4	39	13	9	6	504	9	Matrix
	3	5	**35**	**10**	**9**	**6**	**498**	**9**	Matrix: garnet rim
	4	5	**22**	**3**	**9**	**6**	**471**	**15**	Inclusion: garnet
	5	5	**22**	**8**	**9**	**4**	**471**	**10**	Inclusion: garnet
	6	3	26	12	9	6	481	13	Inclusion: garnet
	7	5	**27**	**4**	**9**	**5**	**483**	**10**	Inclusion: garnet
SPH99-3	1	10	38	11	9	3	502	5	Matrix: garnet rim
	2	10	**33**	**9**	**9**	**3**	**494**	**6**	Matrix: garnet rim
	3	10	38	14	9	3	502	5	Inclusion: garnet
	4	2	**24**	**3**	**7**	**1**	**477**	**3**	Matrix: garnet rim
	5	5	20	9	7	4	463	11	Matrix
	6	3	**27**	**6**	**7**	**3**	**482**	**7**	Matrix: garnet rim
	7	4	**15**	**5**	**7**	**2**	**450**	**6**	Inclusion: garnet
	8	3	**13**	**2**	**7**	**1**	**445**	**4**	Inclusion: garnet
SPH99-5	1	3	**31**	**11**	**13**	**7**	**489**	**13**	Inclusion: garnet rim
	2	3	**22**	**10**	**13**	**6**	**467**	**17**	Inclusion: garnet rim
	3	3	**31**	**11**	**13**	**6**	**488**	**13**	Inclusion: garnet core
	4	4	23	15	13	7	462	24	Matrix
	5	3	**43**	**9**	**13**	**5**	**508**	**8**	Matrix
	6	4	41	18	13	9	501	17	Inclusion: garnet
	7	3	**38**	**11**	**13**	**6**	**502**	**10**	Inclusion: garnet
	8	1	29		13		488		Matrix
SPH99-7	1	7	**14**	**7**	**13**	**3**	**456**	**11**	Inclusion: garnet
	2	2	**23**	**4**	**13**	**3**	**462**	**20**	Inclusion: garnet
	5	7	**20**	**8**	**7**	**3**	**464**	**8**	Inclusion: garnet
	6	8	28	11	7	4	481	8	Inclusion: garnet
	7	7	**26**	**6**	**7**	**2**	**479**	**5**	Inclusion: garnet
	8	8	**18**	**6**	**7**	**2**	**460**	**6**	Inclusion: garnet
SPH99-8a	1	2	**24**	**7**	**13**	**5**	**476**	**12**	Inclusion: garnet
	3	3	44	26	13	15	505	22	Inclusion: garnet
	4	4	**38**	**13**	**13**	**6**	**500**	**12**	Matrix: garnet rim
	5	6	**37**	**13**	**13**	**5**	**499**	**9**	Matrix
SPH99-8b	6	6	32	18	13	7	487	12	Matrix: garnet rim
	7	2	**14**	**10**	**13**	**7**	**444**	**26**	Inclusion: garnet
	10	6	32	18	13	7	486	14	Matrix
	11	4	**30**	**9**	**13**	**5**	**488**	**9**	Matrix
	12	5	**18**	**5**	**13**	**2**	**460**	**6**	Matrix
SPH-148a	1	2	26	17	13	12	459	19	Inclusion: garnet
	4	2	**22**	**9**	**13**	**6**	**477**	**18**	Inclusion: garnet
	5	3	**22**	**3**	**13**	**2**	**477**	**24**	Inclusion: garnet
	6	3	**24**	**5**	**13**	**3**	**477**	**16**	Inclusion: garnet
SPH-148c	1	3	17	12	9	7	450	21	Inclusion: garnet
	2	3	14	13	9	7	433	32	Inclusion: garnet
	3	2	**40**	**5**	**9**	**3**	**505**	**5**	Inclusion: garnet
	4	5	24	16	9	7	460	26	Inclusion: garnet
	5	2	15	11	9	8	446	29	Inclusion: garnet
SPH-149c	1	4	**22**	**8**	**13**	**4**	**470**	**10**	Inclusion: garnet
	2	5	**15**	**6**	**13**	**3**	**449**	**11**	Inclusion: garnet
	3	4	**15**	**11**	**13**	**6**	**444**	**17**	Inclusion: garnet
	4	7	**21**	**7**	**13**	**3**	**467**	**8**	Inclusion: garnet
	5	5	**24**	**10**	**13**	**5**	**474**	**10**	Matrix: garnet rim
	6	3	**23**	**5**	**13**	**3**	**474**	**7**	Matrix
	7	4	**19**	**8**	**13**	**4**	**464**	**15**	Inclusion: garnet

Table 2 continued

1	2 Grain	3 No. of spots[a]	4 Zr ppm	5 1σ (SD) [b]	6 Exp. SD [c]	7 1σ SE	8 *T* (°C)	9 1σ (SE)[d]	10 Notes
SPH-149d	1	27	**33**	**7**	**7**	**1**	**493**	**2**	Matrix
	2	11	**36**	**6**	**7**	**2**	**499**	**3**	Inclusion: garnet
	3	7	**34**	**5**	**7**	**2**	**496**	**3**	Inclusion: garnet
	4	12	33	8	7	2	492	4	Martix: garnet rim
	5	7	**34**	**4**	**7**	**2**	**496**	**3**	Matrix: pseudomorph
	6	8	31	8	7	3	490	5	Matrix: pseudomorph
	7	86	30	9	7	1	486	2	Matrix
	8	62	**34**	**7**	**7**	**1**	**496**	**2**	Matrix
e	9	1	35.8		1		497	1.5	Matrix
e	10	1	36.4		1		498	1.5	Matrix
SPH-150	1	4	25	18	7	9	470	18	Inclusion: garnet margin
	2	1	29		7		486		Inclusion: garnet core
	3	4	**23**	**4**	**7**	**2**	**473**	**6**	Inclusion: garnet core
	4	3	**23**	**7**	**7**	**4**	**472**	**9**	Inclusion: garnet core
	5	4	32	12	7	6	491	10	Inclusion: garnet core
	6	4	**27**	**3**	**7**	**2**	**482**	**4**	Matrix: garnet rim
	7	2	**22**	**1**	**7**	**1**	**472**	**1**	Matrix
	8	5	34	8	7	3	496	5	Matrix

[a]Number of analyses = no. of spots × 4 (four simultaneous spectrometer analyses)

[b]SD is standard deviation (measured) of all analyses for a grain. Compare with expected SD to ascertain homogeneity of grain. Statistically homogeneous grains are indicated in **bold** text

[c]Expected standard deviation calculated from Poisson statistics for three analysis protocols: ± 13 ppm = 100 nA and 120 s; ± 9 ppm = 200 nA and 120 s; ± 7 ppm = 200 nA and 200 s

[d]SE = standard error (measured) of all temperatures determined on a single grain (= std dev/$\sqrt{N}$)

[e]Analyses by SIMS. All other analyses are by electron microprobe

at 500°C and 3.5°C at 450°C with a low temperature detectability of approximately 340°C. Ion probe analyses carry higher precision and are both time and cost effective. However, high spatial resolution is required for many of the analyses reported here, especially small inclusion grains.

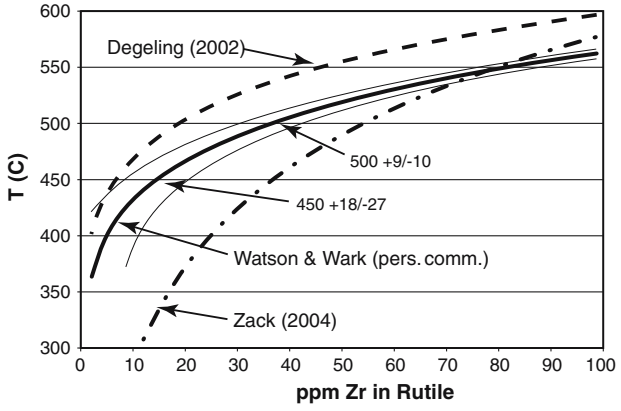

Fig. 2 Plot of Zr concentration (ppm) versus temperature (°C) for three calibrations of the Zr-in-rutile thermometer (Degeling 2002; Zack et al. 2004; Watson et al. 2006). *Thin solid line* shows propagated temperature uncertainty based on the analytical precision of ca. 7 ppm from the electron microprobe procedure adopted for this study

Results

Five hundred seventeen spots from 76 rutile grains in 12 samples from nine outcrops were analyzed and the results are listed in Table 2. The table lists the number of spots analyzed on each grain, the average Zr concentration in the grain, the standard deviation of this average concentration, and the expected standard deviation based on counting statistics in columns 3–6. Comparison of the measured to the expected standard deviations provides a measure of the homogeneity of a grain. Grains in which the measured standard deviation is less than or equal to the expected standard deviation are indicated in bold face, and a number of other grains are very close to this criteria (with the small sampling of some grains the statistics are not very robust). As can be seen from Table 2, most rutile grains analyzed are statistically homogeneous, and in nearly all grains the measured standard deviation is within a few ppm of the expected standard deviation. For these homogeneous rutile grains, the standard error (SE—column 7) provides a measure of the precision of the mean composition, and the temperature calculated from this mean composition (columns 8–9). Most grains have calculated temperature uncertainties (SE of Table 2,

column 9) better than ± 15°C, and more than half are better than ± 10°C.

Before attempting to interpret the temperatures calculated from the Ti thermometer, the nature of Zr distribution within individual rutile grains from these samples must be assessed. Sample SPH-149d contains rutile crystals sufficiently large that the zoning of Zr could be measured. The three crystals illustrated in Fig. 3 all seemingly have systematic distributions of Zr, although the distribution is not the same in each. Grain 1 (Fig. 3a) shows what appears to be roughly concentric zoning with the lowest Zr concentrations in the core. The other two grains (7 and 8; Fig. 3b, c) have zoning patterns that are far less regular. Although it is tempting to interpret the concentric zoning observed in grain 1 as growth zoning, careful consideration of the precision of these data do not warrant such an interpretation. As can be seen in Table 2, grains 1, 7, and 8 have been analyzed for 27, 86, and 62 spots, respectively. The measured standard deviations of these independent spot analyses are 7, 9, and 7 ppm, respectively, compared with the expected standard deviation of 7 ppm. Grains 1 and 8 (Fig. 3a, c) are clearly statistically homogeneous, and grain 7 (Fig. 3b) nearly so. Therefore, the roughly concentric pattern observed in grain 1 (Fig. 3a) cannot be interpreted as statistically meaningful and it must be concluded that these grains are all homogeneous within analytical uncertainty.

The two SIMS analyses were performed on grains from this same sample (SPH-149d), although not the same grains as were analyzed by electron probe. The temperatures obtained (497 and 498°C, respectively) overlap those obtained from electron microprobe analyses (486 ± 2 to 499 ± 3°C; Table 2).

Analysis of rutile grains in all of the different textural settings in which it occurs is a goal of this study, and large area X-ray maps of Ti were used for this purpose, as discussed above. Figure 4 shows an example of such a map from sample SPH99-1c. In practice the X-ray map was overlain on either the optical or BSE image of the area, the rutile crystals identified and then located on the microprobe using BSE. In the metapelites, rutile occurs as inclusions in garnet as well as in the matrix. In the metabasites, rutile occurs inside of garnet whereas only sphene occurs in the matrix. In one metapelite sample (SPH-149d), rutile occurs in prismatic pseudomorphs along with zircon, magnetite, and silicate minerals (Fig. 5a, b).

Figure 4a shows the distribution of temperatures calculated for rutile grains in sample SPH99-1c. Temperatures for grains within garnet range from 460 ± 10 to 475 ± 11°C whereas matrix crystals record temperatures of 463 ± 9 to 505 ± 7°C. Although in several samples, rutile crystals in the matrix have temperatures similar to crystals within garnet, in all cases the highest temperatures are in matrix rutile crystals. This observation strongly suggests progressive growth of rutile with increasing temperature, most likely by continuous reaction with other Ti-bearing phases. Furthermore, it is significant to note that the maximum temperature

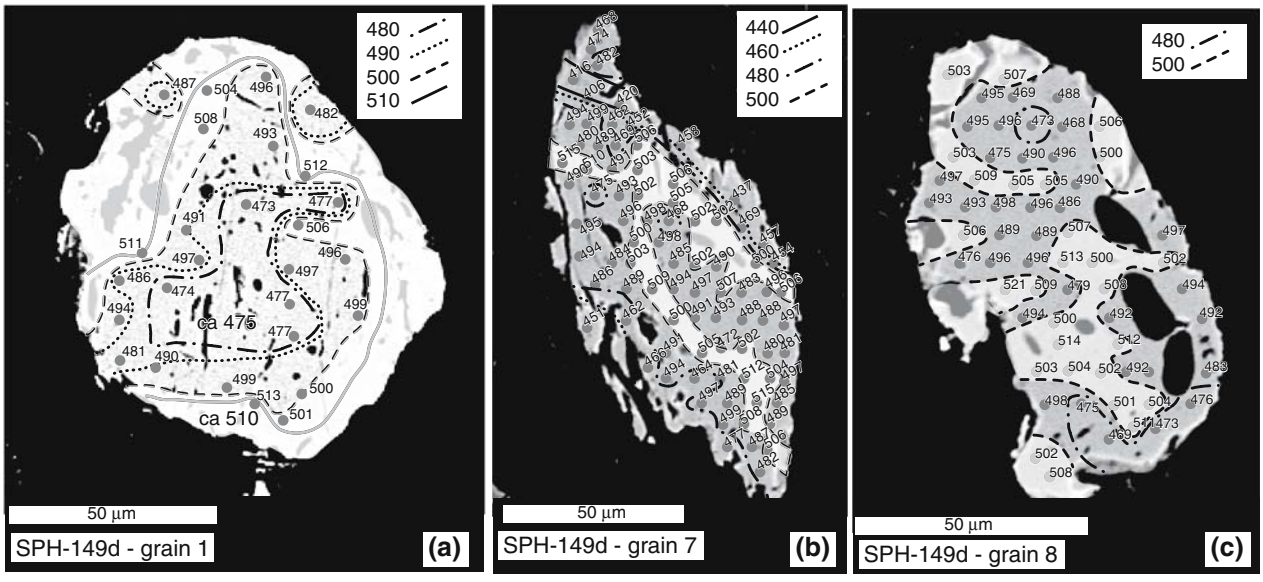

Fig. 3 Backscattered electron images of three (**a**–**c**) rutile crystals from sample SPH-149d (see Fig. 1 for location). *Gray spots* show locations of analysis points (spot size is ca. 2 µm). Numbers are temperatures calculated from rutile thermometer (calibration of Watson et al. 2006). Temperatures are contoured as indicated. For ease of visualization, the regions of the crystals that record temperatures in excess of 500°C are *highlighted*

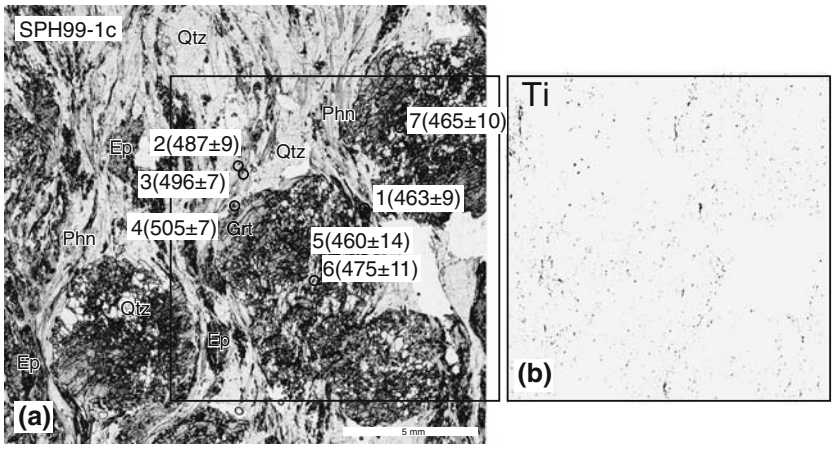

Fig. 4 **a** Photomicrograph of a part of sample SPH99-1c showing locations of rutile crystals (*circles*), grain numbers and calculated temperatures. **b** X-ray map showing distribution of Ti in a part of sample SPH99-1c (see box in **a** for location). Maps such as these were used to locate accessory phases. Abbreviations as in Table 1

recorded by rutile inclusions within garnet provides a minimum temperature for the growth of the garnet that surrounds it. Although there is some variation from sample to sample, the temperatures of rutile inclusions within garnet suggest that garnet growth commenced around 475°C and continued until around 500°C.

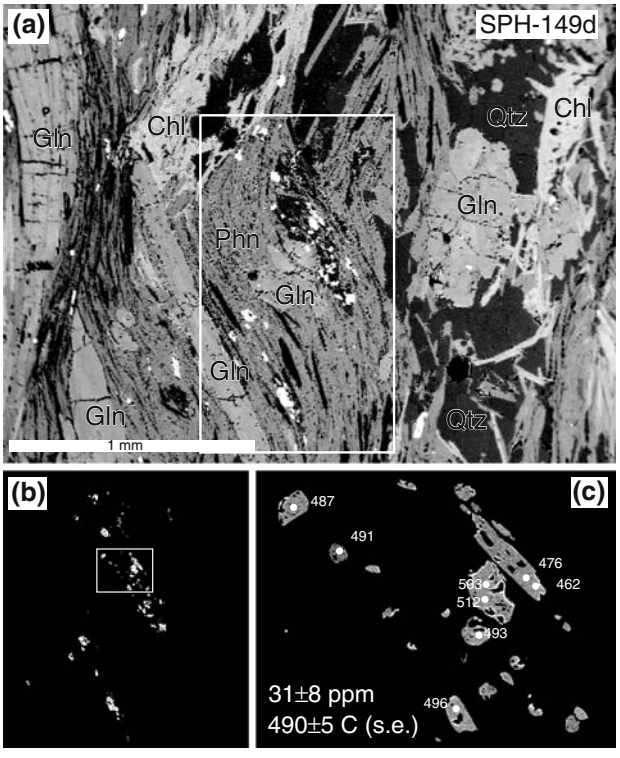

Fig. 5 Images showing rutile-bearing pseudomorph (?) texture. **a** BSE image showing two elongated regions that contain numerous rutile crystals. *Box* shows area of **b**. **b** High contrast BSE image showing distribution of rutile crystals in suspected pseudomorphs. Note how crystals define areas suggestive of a prismatic precursor. *Box* shows area of **c**. **c** Enlargement of area in **b** showing analysis spots and temperatures calculated from rutile thermometry. Abbreviations as in Table 1

Several lines of evidence including (1) the homogeneity of Zr concentrations within individual rutile grains, regardless of size; (2) the similarity of temperatures recorded by grains in similar textural settings; and (3) the systematics of temperature differences between rutile inclusions and matrix grains all suggest that the temperatures recorded by these rutile crystals reflect the temperature at which the crystal grew. However, it is necessary to consider whether diffusion could have significantly modified the Zr concentration and thus affected the calculated temperature. Watson et al. (2006) quote unpublished diffusivity of Zr in rutile to be $D = 9.77 \times 10^{-15} \exp(-171{,}000)/RT)$ in units of m^2/s and J/mole. At 500°C the expected diffusivity of Zr in rutile would be 2.7×10^{-26} m^2/s which corresponds to a characteristic diffusion distance in 1 m.y. ($= \sqrt{Dt}$) of approximately 1 μm. Although the total amount of time spent by the samples near the metamorphic peak temperature of ca. 500°C is not known, it was likely to have been less than a few 10 s of m.y., so the integrated characteristic diffusion distance is not likely to have exceeded 10 μm and therefore it is not likely that diffusion has modified the distribution of Zr in rutile subsequent to its growth.

In several samples of metapelite, small rutile crystals were identified along with other oxides and silicates in a pattern that suggests a pseudomorph (Fig. 5). The mean Zr concentration of all spots (31 ppm) has a standard deviation of ± 8 ppm, which is very close to the expected deviation of ± 7 ppm, suggesting that the Zr concentration in these crystals is uniform. This, in turn, suggests that the crystals were produced at the same time by a single reaction, presumably the reaction that produced the pseudomorph, at a temperature of 490 ± 5°C (1 SE of the mean). Unfortunately, the identity of the proposed pseudomorphed crystal has not been determined, but it might be possible to do so in future studies of lower grade metapelites.

Figure 6 depicts the array of Ti in rutile temperatures from northern Sifnos, which range from 433 to 508°C with a mean of 477 ± 18°C. The range of temperatures encountered within a single grain (e.g. Fig. 3) as well as the comparison of observed temperatures with expected variation from Poisson statistics suggests that the temperature variation reflects continuous rutile growth over an approximately 50° temperature interval. No systematic geographic variation of either the minimum or maximum Zr-in-rutile temperature is observed, suggesting that the Sifnos blueschists were metamorphosed as a coherent block, consistent with inferences of previous workers (e.g. (Matthews and Schliestedt 1984; Schliestedt 1986; Schliestedt and Matthews 1987; Schliestedt et al. 1987).

Previous estimates of metamorphic temperatures from Sifnos are 440–600°C (P = 12–18 kbar) (Matthews and Schliestedt 1984; Schliestedt 1986; Schliestedt and Matthews 1987; Trotet et al. 2001b; Schmädicke and Will 2003). Indeed, Schliestedt (1986) inferred a peak metamorphic temperature of 475 ± 25°C based on Fe–Mg partitioning between garnet and pyroxene from Vroulidia Bay (Fig. 6), which is statistically indistinguishable from the results of the rutile thermometry using the Watson et al. (2006) calibration. Matthews and Schliestedt (1984) reported quartz–rutile oxygen isotope temperatures of ca. 440–510°C, precisely the range found here for Zr in rutile thermometry, supporting the conclusion that rutile grew over a range of temperatures.

The higher temperatures inferred by Trotet et al. (2001b) and Schmädicke and Will (2003) of 580 ± 25 and 600 ± 25°C, respectively, are not reflected in the rutile crystallization or the oxygen isotope temperatures. There are several possible explanations for this apparent discrepancy. First, the higher temperatures could be incorrect as a result of inaccuracies in the thermodynamic data used (Berman 1988; Holland and Powell 1998, respectively), the limitations of the activity models employed for amphiboles, pyroxenes, micas and chlorite, or because the natural samples crystallized at an activity of H_2O less than unity as assumed in the calculations. Second, it is possible that the pressure correction noted by Degeling (2002) should be applied to the Sifnos rocks. The Watson et al. calibration was done at 1.0 GPa whereas the pressure of the Sifnos blueschists has been estimated to be 1.5 ± 0.3 GPa (Schliestedt 1986). A correction of 0.2–0.8 GPa (over the nominal 1.0 of the experimental calibration) would increase the calculated temperatures by ca. 10–40°C, which would reduce the discrepancy, but not eliminate it.

Another possibility is that the peak temperature actually was considerably higher (e.g. 600°C) than highest measured Zr-in-rutile temperature (i.e. 505°C). The consistency of the rutile temperatures with both major phase thermometry (Schliestedt 1986) and oxygen isotope thermometry (Matthews and Schliestedt 1984) supports our favored interpretation that the peak temperature is on the order of 505 ± 10°C.

The reactions by which rutile grew are difficult to ascertain. In no sample was a Ti-rich precursor to rutile identified. Sphene was found in the metabasite samples, but was restricted to the matrix whereas rutile was found inside garnet. Although the exact reaction producing rutile is not known, it is well known that in the TiFAS system, ilmenite is replaced by rutile with increasing pressure. For example, the so-called GRAIL reaction:

$$\underset{\text{rutile}}{3TiO_2} + \underset{\text{almandine}}{Fe_3Al_2Si_3O_{12}} = \underset{\text{ilmenite}}{3FeTiO_3} + \underset{\text{kyanite}}{Al_2SiO_5} + \underset{\text{quartz}}{2SiO_2}$$

has a flat P–T slope and occurs at around 1.2 GPa in the TiFAS system. Addition of other components to the garnet lowers the pressure of equilibration, and pressures of 0.8–1.0 are typical for metapelite garnets from blueschists.

Assuming that ilmenite is the precursor to rutile, then the Zr-in-rutile temperatures reflect the temperature at which this, or a similar, reaction was crossed, adjusted for the appropriate bulk composition. If one assumes the pressure of rutile formation and correlates this pressure with a measured temperature of rutile formation, one can obtain a point on the rock's P–T path that can be used to calculate an instantaneous

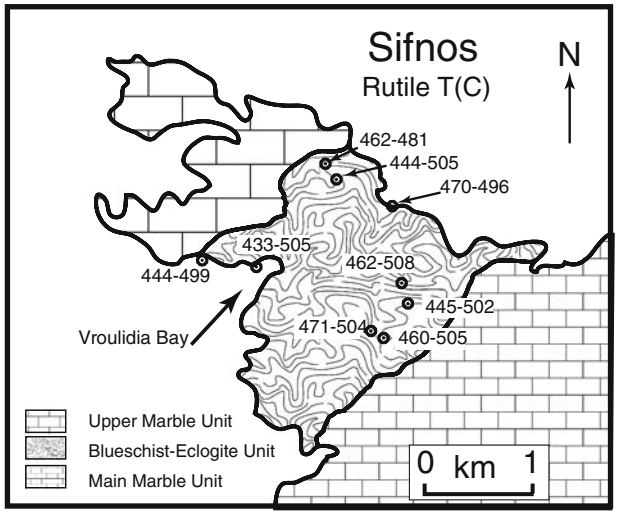

Fig. 6 Map of northern Sifnos showing the range of temperatures for all grains from each sample calculated from Zr-in-rutile thermometry

geothermal gradient. Taking 1.0 GPa for the minimum pressure of rutile formation and correlating this pressure with the minimum temperature of rutile formation (i.e. 450°C), one arrives at approximately 13 deg/km. This is a relatively shallow geothermal gradient for a subduction complex and implies either (1) subduction was slow or (2) subduction was shallow allowing an approach to thermal equilibration. Assuming the metamorphic peak to have been 505°C at 1.5 GPa, a *P–T* path with a slope of approximately 3 deg/km is implied ($\Delta T/\Delta$depth = 55°/17 km). This rather steep slope requires either (1) an increase in the rate of subduction or (2) a steepening of the angle of subduction.

The above discussion is somewhat speculative, but unless rutile is produced by a mechanism other than ilmenite breakdown, then the magnitude of the calculations is expected to be correct. Most importantly, the above discussion points to the enormous potential of rutile thermometry, once the reactions that produce rutile are better understood. Coupled with precise age determinations, Zr-in-rutile thermometry has the potential to provide a *P–T–t* point for a subduction complex, which would go a long way towards improving our understanding of subduction tectonics.

Conclusions

Zr-in-rutile thermometry applied to blueschists from Sifnos yields systematic results suggestive of an approach to chemical equilibrium indicating that the temperatures obtained reflect temperatures of rutile crystallization. Electron microprobe analysis can achieve precisions of ca. ± 7 ppm on a single spot, which equates to temperature uncertainties of + 18/–27 at 450°C, decreasing to + 9/–10 at 500°C, and ion microprobe analyses have a precision of ± 1 ppm, which equates to a temperature uncertainty of ± 3.5 to ± 1.5, respectively. This precision is sufficient to differentiate different generations of rutile in these samples. Inasmuch as many major-phase reactions in blueschists are relatively insensitive to temperature, application of Zr-in-rutile thermometry with pressure sensitive reactions has the potential of yielding precise *P–T* conditions of subduction zone metamorphism. Of particular importance is both the highly precise nature of the Ti in rutile temperatures of ± 10°C or less compared to major element exchange thermometers (± 25°C) and the ease with which they can be obtained by relatively standard EMP procedures.

The results of this study are consistent with the blueschist facies rocks of northern Sifnos having crystallized with a peak metamorphic temperature near 510°C, consistent with the findings of previous workers. These results suggest that the Zr-in-rutile thermometer is sufficiently precise to enable fine-scale distinction between different blueschist blocks, such as are found on the neighboring island of Syros, and which will be the subject of a future contribution.

Acknowledgments This work was funded by grants from the National Science Foundation 0337413 (Spear), 0409622 (Wark and Spear), and 0320995 (Spear, Wark and Watson). Amherst College research funds (Cheney) supported the collecting and shipping samples from Sifnos. We much appreciated the good humor and support of Captain Niko from Kini, Syros, who provided boat transportation and much interesting scenery on numerous occasions.

References

Avigad D (1993) Tectonic juxtaposition of blueschists and greenschists in Sifnos Island (Aegean Sea)—implications for the structure of the Cycladic Blueschist Belt. J Struct Geol 15:1459–1469

Berman RG (1988) Internally-consistent thermodynamic data for minerals in the system Na_2O–K_2O–CaO–MgO–FeO–Fe_2O_3–Al_2O_3–SiO_2–TiO_2–H_2O–CO_2. J Petrol 29:445–522

Blake MC Jr, Bonneau M, Geyssant J, Kienast JR, Lepvrier C, Maluski H, Papanikolaou D (1981) A geologic reconnaissance of the Cycladic blueschist belt, Greece. Geol Soc Am 92:247–254

Degeling HS (2002) Zircon equilibria in metamorphic rocks. Australian National University, Canberra

Forster MA, Lister GS (2005) Several distinct tectono-metamorphic slices in the Cycladic eclogite-blueschist belt, Greece. Contrib Mineral Petrol 150:523–545

Holland TJB, Powell R (1998) An internally-consistent thermodynamic dataset for phases of petrological interest. J Metamorph Geol 16:309–343

Lister GS, Raouzaios A (1996) The tectonic significance of a porphyroblastic blueschist facies overprint during Alpine orogenesis: Sifnos, Aegean Sea, Greece. J Struct Geol 18:1417–1435

Matthews A, Schliestedt M (1984) Evolution of the blueschist and greenschist facies rocks of Sifnos, Cyclades, Greece. Contrib Mineral Petrol 88:150–163

Okrusch M, Bröcker M (1990) Eclogite facies rocks in the Cycladic blueschist belt, Greece: a review. Eur J Mineral 2:451–478

Schliestedt M (1986) Eclogite–blueschist relationships as evidenced by mineral equilibria in the high-pressure metabasic rocks of Sifnos (Cycladic Islands), Greece. J Petrol 27:1437–1459

Schliestedt M, Matthews A (1987) Transformations of blueschist to green facies rocks as a consequence of fluid infiltration, Sifnos (Cyclades) Greece. Contrib Mineral Petrol 97:237–250

Schliestedt M, Altherr R, Matthews A (1987) Evolution of the Cycladic crystalline complex: petrology, isotope geochemistry and geochronology, NATO Advanced Study Institutes Series. Series C. In: Helgeson HC (ed) Chemical transport in metasomatic processes. Reidel Publishing, Dordrecht, pp 389–428

Schmädicke E, Will TM (2003) Pressure–temperature evolution of blueschist facies rocks from Sifnos, Greece, and implications for the exhumation of high-pressure rocks in the Central Aegean. J Metamorph Geol 21:799–812

Trotet F, Jolivet L, Vidal O (2001a) Tectono metamorphic evolution of Syros and Sifnos islands (Cyclades, Greece). Tectonophysics 338:179–206

Trotet F, Vidal O, Jolivet L (2001b) Exhumation of Syros and Sifnos metamorphic rocks (Cyclades, Greece). Eur J Mineral 13:901–920

Watson EB, Wark DA, Thomas JB (2006) Crystallization thermometers for zircon and rutile. Contrib Mineral Petrol 151:413–433

Wijbrans JR, van Wees JD, Stephenson RA, Cloetingh SAPL (1993) Pressure–temperature time evolution of the high pressure metamorphic complex of Sifnos Greece. Geology 21:443–446

Zack T, Moraes R, Kronz A (2004) Temperature dependence of Zr in rutile: empirical calibration of a rutile thermometer. Contrib Mineral Petrol 148:471–488